# High-Performance Control for a Permanent-magnet Linear Synchronous Generator Using State Feedback Control Scheme Plus Grey Wolf Optimization

Xiaodong Sun[1], Minkai Wu[1], Zebin Yang[2], Gang Lei[3*], and Youguang Guo[3]

[1]Automotive Engineering Research Institute, Jiangsu University, Zhenjiang 212013, China
[2]School of Electrical and Information Engineering, Jiangsu University, Zhenjiang, China
[3]School of Electrical and Data Engineering, University of Technology Sydney, NSW 2007, Australia
[*]gang.lei@uts.edu.au

**Abstract: This paper proposes an optimal control scheme for a permanent-magnet linear synchronous generator (PMLSG) using the state feedback control method plus the grey wolf optimization (GWO) algorithm. First, A novel state-space model of linear PMLSG is established in order to obtain desired dynamics and enough power when used for the smooth wave energy. Second, the GWO algorithm is adopted to acquire weighting matrices Q and R in the process of optimizing linear quadratic regulator (LQR). What is more, a penalty term is brought into the fitness index to reduce the overstrike of output voltage and keep the rate of work more stable. Finally, optimal LQR-based state feedback controlled (SFC) with and without penalty term and PI controllers are compared both in simulations and in experiments. Results clearly prove that the proposed optimal control strategy performs a better response when compared to other strategies.**

**Index terms- permanent magnet linear synchronous generator, wave energy, state-space model, grey wolf optimization, linear quadratic regulator**

## 1. Introduction

### *1.1. Aim and Difficulties*

With the global decline in fossil energy, making full use of new energy has become more and more important. Compared to wind and solar energy, wave energy density is the highest. Wave energy refers to the kinetic and potential energy of ocean surface waves, which has huge power. In the face of the advantages of small energy loss and high density, the wave energy is considered as an alternative to conventional power generation. Energy conversion device plays a significant role in the process of generation. Compared with the rotational permanent-magnet generator [1], the linear permanent-magnet generator has obvious superiority such as less transmission loss, no excitation current, simple structure and high generation efficiency [2]-[7]. Linear motors can be divided into many categories, such as the permanent magnet type, magnetic resistance type, induction type and so on. The performance of motor optimization can be generally divided into two aspects. One is the optimization of motor design, the other is the optimization of motor control [8]-[11]. Multi-objective design and optimization are the major research hotspots. This paper focuses on the optimization of PMLSG control with a MIMO nonlinear state-space. It is crucial to improve the performance of generation for PMLSG with stable voltage output.

### *1.2. Review*

In the power generation stage, the control system adopts the control algorithm of voltage loop and current loop structure. This control scheme has become an extensive generator control strategy due to simple structure, fast response and good robustness. However, the drawback of double PI loop is obvious that the control performance may be affected by controller parameters. Recently, in the area of the intelligent control, some nature-inspired algorithms are employed widely to optimize the parameters of PI controller. In [12]-[15], the Particle Swarm Optimization algorithm (PSO) is employed to improve the efficiency and decrease the losses online. Meanwhile, the PSO algorithm has been improved to adapt the learning rates of the recurrent functional link (FL)-based fuzzy neural (FNN) online. Moreover, In [16] and [17], as one of the most popular swarm intelligence approaches, the artificial bee colony (ABC) algorithm is employed into LQR controller optimization for inverted pendulum control. The comparative results show that ABC algorithm has higher performance over the genetic algorithm (GA) and PSO algorithm. In [18], the GA is combined with motion cueing algorithm (MCA) to improve the developed LQR to obtain the best weighting matrices. The GA-based optimal MCA can use the workspace more efficiently, which is reliable, stable and effective in the application. The mentioned powerful algorithms have been widely applied in the fact. However, PSO algorithm is easy to fall into the local optimal for the discrete optimization problem is not well handled. As for the ABC algorithm, the search scope is not comprehensive enough, and it is easy to fall into local optimization for a long time. For GA, the local search ability is poor, which leads to the time consuming simple genetic algorithm and low search efficiency in the late evolution. In practical application, genetic algorithm is easy to produce premature convergence problem. The references presented above with intelligent algorithms employ the fitness function similarly. The fitness function is vital during the iteration process, and has a crucial effect on the nature of controller. The parameters of designed controller may not be proper for different conditions. In order to keep the result satisfying, the fitness function must be amended (for example, overshoots reduction). As a result, the fitness function mentioned above needs to add a penalty term. When the undesired phenomenon happens, the term will be punished severely by increasing obviously its fitness value. Hence, the weighting matrices that may cause overshoots will be useless

in the iteration cycle. The grey wolf optimization (GWO) is used in the proposed SFC, which belongs to one of the natural-inspired optimization algorithms, put forward by Mirjalili [19] and [20]. An efficient PMSM speed controller based on Grey Wolf Optimization (GWO) algorithm is proposed to reduce speed ripple at low speed operation [21]. The optimization process of GW optimizer in real-time working conditions is explored to ensure satisfactory dynamics. Compared with other powerful algorithms, grey wolf algorithm has better performance in dealing with the optimal problems. it is more robust and exhibits faster convergence, furthermore, it requires fewer parameters for adjustment and less operators compared to other evolutionary approaches, which is an advantage when rapid design process is considered. These proprieties are particularly important from the point of view of real time implementation. The GWO reveals the superiority in simple calculation, precise solution, convergence independence of initial conditions and able to handle local minima, especially iterations in the latter periods [22]. The performances involved in above are important in particular at parameter optimization procedure.

Several design optimization methods for electrical drive systems and permanent magnet motors are involved in [23] and [24]. The state feedback control method may be an appropriate way to combine voltage controller with intelligent algorithm. A state feedback controller (SFC) is employed for a better property with the introduction of disturbance compensation [25]. Nevertheless, coupled with state feedback control, and SFC gain matrix is difficult to determine in the short term. Conventionally, trial-and-error methods are preferred to use for a desired consequence. Different from the Ontology design and electrical drive systems [26], the pole-placement technique can be applied to obtain the best gain matrix, but locating poles properly may be difficult for a complicated system. In [27], it is noted that determining $\boldsymbol{Q}$ and $\boldsymbol{R}$ in linear quadratic regulator (LQR) by an analytic method is proposed to achieve SFC gain matrix. The controller shows good performance for rejecting disturbance. In order to improve system's steady state property, some extra variables will be leaded in the PMLSG model. To ensure zero steady-state voltage error, some integrators are necessary to add to the PMLSG system. In [28] and [29], the state space model of permanent magnet synchronous linear motor has introduced tracking errors [30]. What is proposed about optimal LQR-based DTFC demonstrates perfect control of flux and thrust force with transient response. The added integral variables are the same as the system outputs, and disturbance is rejected in the experimental results.

### 1.3. Contributions and Novelty

The method of state feedback control will be applied to realize the high-performance control for a PMLSG. Furthermore, a method based on GWO and LQR is used to constantly optimal the effect of state feedback control. In this paper, a high-performance control strategy for PMLSG using state feedback control plus Grey Wolf Optimization is proposed, in which the conventional PI voltage loop and current loop structure is compared. The main contributions of this paper are listed as follows.

1)A MIMO nonlinear state-space of PMLSG is given first. Then, a critical step is taken to linearize the model. Integral action of tracking speed and zero *d*-axis current are incorporated in the control scheme by state augmentation of the novel state-space model to reduce the steady-state error. Instead of focusing on inputs and outputs, this modeling approach considers internal variables as well. integrals are drawn into the model to ensure small steady-state error.

2) The state feedback control is the first time to be applied in PMLSG. During the period of control, GWO is implemented to optimal the performance of generating electric. Based on the appearance of overshoot, the penalty term is considered in the proposed objective function minimized by GWO. The GWO algorithm plays an important role in acquiring values of weighting matrices $\boldsymbol{Q}$ and $\boldsymbol{R}$ which are demanded to calculate discrete state feedback voltage controllers by Matlab LQR function.

### 1.4. Paper Layout

The chapters are arranged as follows. In section 2, the dynamic model of PMLSG and linearization of the model are presented. The discrete voltage controller for the linearized PMLSG is given in section 3. The GWO algorithm is summarized in section 4 and section 5 describes the application of GWO to design SFC. Section 6 details simulation result, including evaluation of fitness index, evolution trend of PMLSG direct voltage within different fitness indexes and simulation response at different load resistance. Experimental results are supplied and proposed control approaches are discussed in Sections 7, which is followed by the conclusion.

## 2. Model of PMLSG

The nonlinear state-space dynamic model of the surface mounted PMLSG in *d-q* axis reference mover frame can be written as [20]

$$\dot{\boldsymbol{x}}(t) = \boldsymbol{A}(t)\boldsymbol{x}(t) + \boldsymbol{B}\boldsymbol{u}(t) + \boldsymbol{E}f(t) \tag{1}$$

where

$$\boldsymbol{A}(t) = \begin{bmatrix} -\frac{R_s}{L_s} & n_p\frac{\pi}{\tau}v & 0 \\ -n_p\frac{\pi}{\tau}v & -\frac{R_s}{L_s} & -n_p\frac{\pi\psi}{\tau L_s} \\ 0 & \frac{3n_p\pi\psi}{2\tau M} & -\frac{B_v}{M} \end{bmatrix}, \boldsymbol{B} = \begin{bmatrix} \frac{1}{L_s} & 0 \\ 0 & \frac{1}{L_s} \\ 0 & 0 \end{bmatrix}$$

$$\boldsymbol{E} = \begin{bmatrix} 0 & 0 & -\frac{1}{M} \end{bmatrix}^{\mathrm{T}}, \boldsymbol{x}(t) = \begin{bmatrix} i_d(t) & i_q(t) & v(t) \end{bmatrix}^T,$$

$$f(t) = F_l(t)\ \boldsymbol{u}(t) = \begin{bmatrix} u_d & u_q \end{bmatrix}^{\mathrm{T}}$$

where $i_d$ and $i_q$ are the *d*-axis and *q*-axis current, respectively, $R_s$ and $L_s$ denote the resistance and inductance of stator, respectively, $\Psi$ is the permanent magnet flux linkage, $n_p$ is the number of pole pairs, $v$ is mover speed, $\tau$ is the polar distance, $u_d$ and $u_q$ are the *d*-axis and *q*-axis voltage, respectively, $M$ is the mass of the mover, $B_v$ is viscous friction, and $F_l$ is the force of load.

Since state variable matrix $\boldsymbol{A}$ contains nonlinear portion $v$ in $\boldsymbol{A}(1,2)$, $\boldsymbol{A}(2,1)$, the established model is time-variable. It is a critical step to linearize the model for the following design.

As can be seen the nonlinear elements in variable $\boldsymbol{u}(t)$,

$$\boldsymbol{u}(t) = u_l(t) + u_m(t) \tag{2}$$

where

$$\boldsymbol{u_m}(t)=\begin{bmatrix}u_{md}(t)\\ u_{mq}(t)\end{bmatrix}=\begin{bmatrix}-n_p\dfrac{\pi}{\tau}vL_s i_q\\ n_p\dfrac{\pi}{\tau}v(L_s i_d+\psi)\end{bmatrix} \tag{3}$$

The cross-coupled terms of the voltage equation should be subtracted to obtain the linearized state-space model.

$$\dot{\boldsymbol{x}}(t)=\boldsymbol{A}\boldsymbol{x}(t)+\boldsymbol{B}\boldsymbol{u_l}(t)+\boldsymbol{E}f(t) \tag{4}$$

where

$$\boldsymbol{A}(t)=\begin{bmatrix}-\dfrac{R_s}{L_s} & 0 & 0\\ 0 & -\dfrac{R_s}{L_s} & 0\\ 0 & \dfrac{3n_p\pi\psi}{2\tau M} & -\dfrac{B_v}{M}\end{bmatrix}$$

## 3. SFC Controller Design

The performance indexes of PMLSG are the output voltage and active power. In order to ensure small steady-state error, integrals should be drawn into the model. The state model adds tracking speed and zero *d*-axis current in various load conditions to get the stable direct voltage. The added state variables are as follow:

$$e_v=\int(v-v^{ref})\mathrm{d}t \tag{5}$$

$$e_{id}=\int(i_d-i_d{}^{ref})\mathrm{d}t \tag{6}$$

$$\boldsymbol{x}'(t)=\begin{bmatrix}i_d(t) & i_q(t) & v(t) & e_{id}(t) & e_v(t)\end{bmatrix}^T \tag{7}$$

where $e_{id}$ and $e_v$ are the different integral errors between reference and actual value, respectively.

Taking the internal state into the model, a augment state space equation is built and the load torque is ignored.

$$\dot{\boldsymbol{x}}'(t)=A'\boldsymbol{x}'(t)+B'\boldsymbol{u}_l(t)+j\boldsymbol{r}(t) \tag{8}$$

where

$$\boldsymbol{A'}=\begin{bmatrix}-\dfrac{R_s}{L_s} & 0 & 0 & 0 & 0\\ 0 & -\dfrac{R_s}{L_s} & 0 & 0 & 0\\ 0 & \dfrac{3n_p\pi\psi}{2\tau M} & -\dfrac{B_v}{M} & 0 & 0\\ 0 & 0 & 1 & 0 & 0\\ 1 & 0 & 0 & 0 & 0\end{bmatrix},\ \boldsymbol{B'}=\begin{bmatrix}\dfrac{1}{L_s} & 0\\ 0 & \dfrac{1}{L_s}\\ 0 & 0\\ 0 & 0\\ 0 & 0\end{bmatrix},j=\text{-}1,$$

$$\boldsymbol{r}(t)=\begin{bmatrix}0 & 0 & 0 & v^{ref} & i_d^{ref}\end{bmatrix}^T$$

The control law of the built model can be demonstrated as follow:

$$\boldsymbol{u}(t)=-\boldsymbol{K}_c x'(t)=-\boldsymbol{K}_{cx}\boldsymbol{x}(t)-\boldsymbol{K}_{ce}\boldsymbol{x_e}(t) \tag{9}$$

$$\boldsymbol{x}(t)=\begin{bmatrix}i_d(t) & i_q(t) & v(t)\end{bmatrix}^T$$

$$\boldsymbol{x}_e(t)=\begin{bmatrix}e_{id}(t) & e_v(t)\end{bmatrix}^T$$

where $\boldsymbol{K_c}$ is gain matrix of appropriate dimension for the continuous model.

$$\boldsymbol{K}_c=\begin{bmatrix}\boldsymbol{K}_{cx} & \boldsymbol{K}_{ce}\end{bmatrix}=\begin{bmatrix}K_{cx1} & K_{cx2} & K_{cx3} & K_{ce1} & K_{ce2}\\ K_{cx4} & K_{cx5} & K_{cx6} & K_{ce3} & K_{ce4}\end{bmatrix}$$

The model implemented in dSPACE platform to operate needs to be discretized, therefore the control law is changed.

$$\boldsymbol{u}(n)=-\boldsymbol{K}_d x'(n)=-\boldsymbol{K}_{dx}\boldsymbol{x}(n)-\boldsymbol{K}_{de}\boldsymbol{x}_e(n) \tag{10}$$

where *n* represents discrete sample time index.

$$\boldsymbol{K}_d=\begin{bmatrix}\boldsymbol{K}_{dx} & \boldsymbol{K}_{de}\end{bmatrix}=\begin{bmatrix}K_{dx1} & K_{dx2} & K_{dx3} & K_{de1} & K_{de2}\\ K_{dx4} & K_{dx5} & K_{dx6} & K_{de3} & K_{de4}\end{bmatrix}$$

$\boldsymbol{K_{de}}$ is composed of the discretized $e_{id}$ and $e_v$ which can be achieved through the backward Euler integration algorithm.

$$e_v(n)=e_v(n-1)+Ts\left[v(n)-v^{ref}(n)\right] \tag{11}$$

$$e_{id}(n)=e_{id}(n-1)+Ts\left[i_d(n)-i_d{}^{ref}(n)\right] \tag{12}$$

where *Ts* represents the sampling period.

LQR (linear quadratic regulator), and its object is given in the form of state space in modern control theory of linear system, and the objective function is quadratic function for the object state and control input. LQR optimal design means that the designed state feedback controller $\boldsymbol{K}$ should minimize the quadratic objective function $\boldsymbol{J}$, and $\boldsymbol{K_d}$ is uniquely determined by weight matrix $\boldsymbol{Q}$ and $\boldsymbol{R}$, so the selection of $\boldsymbol{Q}$ and $\boldsymbol{R}$ is particularly important. We have to design an energy function that the optimal control trajectory should minimize.

In ordered to get the most suitable gain matrix, the linear quadratic optimization method is applied. Based on the nonlinear state-space dynamic model of the surface mounted PMLSG in *d-q* axis reference mover frame, the linearized state-space model is obtained. $x_i(n)$ and $u_i(n)$ are state variables from the state equation (8):

$$\boldsymbol{J}=\sum_{n=0}^{\infty}(x_i^T(n)\boldsymbol{Q}x_i(n)+u_i^T(n)\boldsymbol{R}u_i(n)) \tag{13}$$

where $\boldsymbol{Q}$ and $\boldsymbol{R}$ are diagonal and constant symmetric positive definite matrixes. The supposed gain matrix is connected to the linear quadratic optimization. Then, operate simulation of GWO for SFC. LQR is a mean of adjusting state feedback controller. After the operation of LQR, GWO is combined with SFC to restrain overshoot.

## 4. Grey Wolf Optimization

The GWO algorithm derives from the leadership hierarchy and hunting mechanism of grey wolves, which is used into SFC optimization. The social hierarchy is divided into four types such as alpha, beta, delta and omega, which are ranged from high to low. They are behalf of different authorities in a wolf group. The levels are submitted three main steps of GWO, including hunting, chasing, tracking, encircling and attacking the prey.

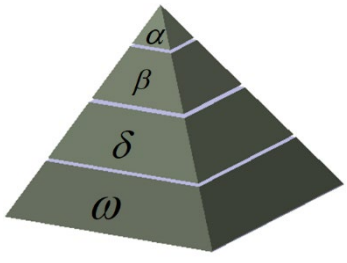


***Fig. 1.*** *Hierarchy of grey wolves*

Fig.1 shows the strict hierarchy of grey wolves in a group. Alphas(α) are consist of a male and a female, which are responsible for sending the hunting command to the

following three levels of wolves. Beta($\beta$) can give assistance to Alpha and command the other lower-level wolves. It plays a role in linking the information between superior and subordinate. Delta($\delta$) wolves are subject to alphas and betas, but they dominate the omega. Each of them has its role, such as scouts, sentinels, elders, hunters, and caretakers. Omega($\omega$) is the last stratum of hierarchy of grey wolves. They make sacrifices for the survival of the team. The main phases of grey wolf hunting are as follows:

1.Tracking, running after, and being close to the prey.

2.Pursuing, encircling, and harassing the prey until it stops moving.

3.Attack towards the prey.

The behavior of encircling the prey can be described by mathematical model.

$$\boldsymbol{D} = |\boldsymbol{C} \times \boldsymbol{X_P}(t) - \boldsymbol{X}(t)| \quad (14)$$

$$\boldsymbol{X}(t+1) = \boldsymbol{X_P}(t) - \boldsymbol{A} \times \boldsymbol{D} \quad (15)$$

where $t$ manifests the real iteration, $\boldsymbol{C}$ and $\boldsymbol{D}$ are coefficient vectors, $\boldsymbol{X_P}(t)$ represents position vector of the prey, and $\boldsymbol{X}$ represents position vector of the grey wolf. The vectors $\boldsymbol{A}$ and $\boldsymbol{C}$ are calculated as follows:

$$\boldsymbol{A} = 2 \times \boldsymbol{a} \times \boldsymbol{r}_1 - \boldsymbol{a} \quad (16)$$

$$\boldsymbol{C} = 2 \times \boldsymbol{r}_2 \quad (17)$$

where $\boldsymbol{a}$ is linearly decreased from 2 to 0 over the course of iterations and $\boldsymbol{r}_1$ and $\boldsymbol{r}_2$ are random vectors in [0, 1].

Fig.2 shows principle of grey wolves hunting. As can be seen, alpha, beta, and delta are the different locations of wolves. The three best solutions are saved firstly, then the other search agents are forced to update their positions so that information can guide the next action.

$$\boldsymbol{D}_\alpha = |\boldsymbol{C}_1 \boldsymbol{X}_\alpha - \boldsymbol{X}|, \boldsymbol{D}_\beta = |\boldsymbol{C}_2 \boldsymbol{X}_\beta - \boldsymbol{X}|, \boldsymbol{D}_\delta = |\boldsymbol{C}_3 \boldsymbol{X}_\delta - \boldsymbol{X}| \quad (18)$$

$$\boldsymbol{X}_1 = \boldsymbol{X}_\alpha - \boldsymbol{A}_1 \boldsymbol{D}_\alpha, \boldsymbol{X}_2 = \boldsymbol{X}_\beta - \boldsymbol{A}_2 \boldsymbol{D}_\beta, \boldsymbol{X}_3 = \boldsymbol{X}_\delta - \boldsymbol{A}_3 \boldsymbol{D}_\delta \quad (19)$$

$$\boldsymbol{X}(t+1) = \frac{\boldsymbol{X}_1 + \boldsymbol{X}_2 + \boldsymbol{X}_3}{3} \quad (20)$$

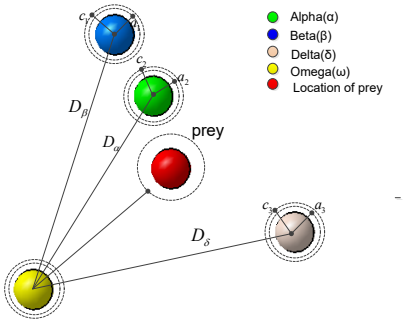


***Fig. 2.*** *Location update of grey wolves hunting*

where $D_\alpha$, $D_\beta$,and $D_\delta$ are final random place vector. $\boldsymbol{X}_1$, $\boldsymbol{X}_2$ and $\boldsymbol{X}_3$ are estimated position command given by alpha, beta and delta, respectively.

As soon as the grey wolves finish the hunting, the attacking goes ahead. When random values of $\boldsymbol{A}$ are not in [-1,1], the GWO algorithm will research globally to find another wolves target. The vector includes random values in [0,2], which is important to improve the reliability of iterations. With the effect of vector $\boldsymbol{C}$, the prey will get harder to discover the wolves in nature.

## 5. Implement of GWO for SFC

### *5.1. Establish of Objective Function*

The objective function affects the weighting matrices with the GWO, so it needs to be determined firstly. And the target function and the control object coexist harmoniously. The proposed function consists of two parts which are the major objective and secondary one depending on their priorities. The linear velocity can reach the aim of satisfied dynamic result, while the output voltage is stable. Keeping zero $d$-axis current and zero overshoot are the secondary control objectives. According to the control objectives suggested above, the proposed objective function can be presented as

$$F_1 = \frac{1}{N}\sum_{n=0}^{N}[|e_{Udc}{}'(n)|nTs + |e_{id}{}'(n)|nTs] \quad (21)$$

Adding the penalty term to the function might restrain overshoot as the result of stabilization.

$$F_2 = \frac{1}{N}\sum_{n=0}^{N}[|e_{Udc}{}'(n)|nTs + |e_{id}{}'(n)|nTs + \eta e_{Udc}{}'(n)nTs] \quad (22)$$

where $e'_{U_{dc}} = U_{dc}(n) - U_{dc}^{ref}(n)$ , $e'_{id}(n) = i_d(n) - i_d^{ref}(n)$, $\eta = \begin{cases} 0 & e'_{U_{dc}} < 0 \\ 10 & e'_{U_{dc}} > 0 \end{cases}$, $U_{dc}{}^{ref}(n)$ is the DC reference voltage and $i_d{}^{ref}(n)$ is the reference current in $d$-axis. The function is divided into three parts which are prime control objective, secondary objective and the penalty term. When the overshoot happens, it needs to be taken as the highest priority option. The coefficient $\eta$ changes from 0 to 10. With the advent of added penalty coefficient, the effect will be learned in the following section.

The flowchart of the GWO algorithm is shown in Fig.3(a) to find optimal controller parameters. Fitness calculation process with GWO iteration making use of formula is shown in Fig.3(b). The optimal solution of control parameter is obtained by the application of LQR and GWO. There are two cut-off conditions to guarantee optimal solution. On the one hand, when the iterations of GWO reach the maximum iterations, the algorithm will finish. On the other hand, when the objective function minimizes, the process of fitness calculation will also finish. With the increase of iterations, the output voltage curve gets more and more better. It can be concluded into four steps.

Step1: produce weighting matrices $\boldsymbol{Q}$ and $\boldsymbol{R}$ randomly.

Step2: acquire the gain matrices $\boldsymbol{K_d}$ by using matlab LQR function.

Step3: take the place of the gain matrices in Simulink and simulate the motor power to obtain data to verify the objective function.

Step4: calculate the fitness.

### *5.2. Bandwidths of Current and Speed Loop*

The bandwidth is defined in terms of the closed-loop frequency characteristic, which represents the maximum frequency at which a system can track the input sinusoidal signal. By general definition, the frequency at which the output decays to 0.707 is called the system's bandwidth. Therefore, the wider the bandwidth is, the stronger the ability of the output of the motor control system to follow the input instructions is. The dynamic performance of the system will get better. The simplified transfer function of the current loop closed-loop system is obtained by reducing the order of state feedback controller.

$$G_{cl} = \frac{1}{2T_s s^2 + 2T_s s + 1} \quad (23)$$

where $T_s$ is sampling period of the current sensor. The smaller frequency value corresponding to amplitude-frequency characteristic -3dB and phase-frequency characteristic -45° is usually taken as the cut-off frequency of the current loop closed-loop system.

$$f_{cb} = \frac{\sqrt{3}-1}{4\pi T_s} \quad (24)$$

where $f_{cb}$ is cut-off frequency which is equal to bandwidth.

The feedback current is obtained by current sensor and sampling period of current sensor is set $5\times10^{-4}$ s. In addition, the various speed is obtained by position signal and sampling period of position sensor is set $5\times10^{-5}$ s. Therefore, the closed loop band-widths of these two loops differ at least a factor of ten.

### 5.3. Lyapunov Stability Analysis

The closed-loop control system with the state feedback control is globally exponentially stable.

Proof: Define a Lyapunov function $V(u(t))$ as

$$V(u(t)) = u(t)^T u(t) = \|u(t)\|^2 \geq 0 \quad (25)$$

The time derivative of the Lyapunov function $V(u(t))$ can be given by

$$\dot{V}(u(t)) = 2u(t)^T \dot{u}(t) = -K_{cx} x^2(t) - K_{ce} x_e^2(t) \leq 0 \quad (26)$$

Thus, the equilibrium point $u(t)$=0 is globally and exponentially stable. $V(u(t))$ has first continuous derivative for all $u(t)$ and $V(u(t))$ is positive definite. As the derivation of $V(u(t))$ is negative semidefinite, the control system is stable. $u(t)$=0 converges to zero exponentially as time goes to infinity.

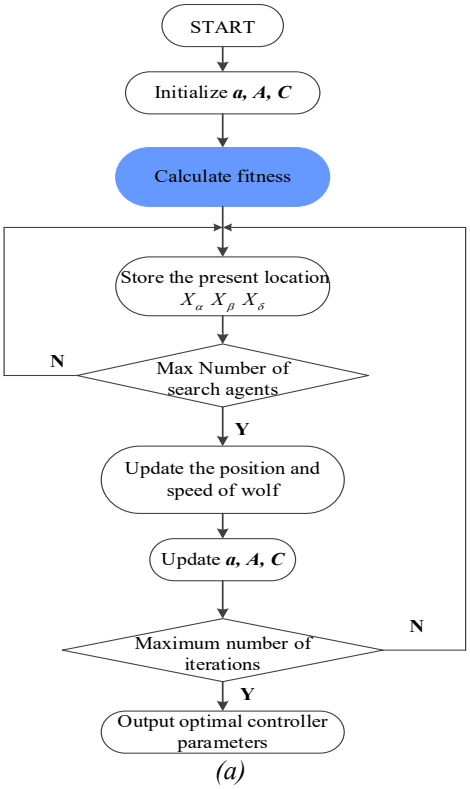


(a)

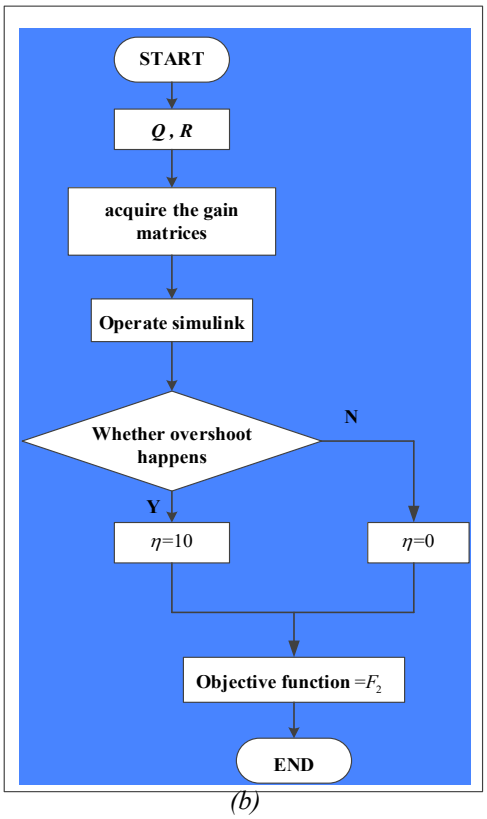


(b)

***Fig. 3.*** ***(a)*** *Flowchart of the proposed GWO algorithm,* ***(b)*** Process of fitness calculation with $F_2$

## 6. Simulation Results

In this part, the optimal LQR-based state feedback controller (SFC) with and without penalty term and PI controller are compared both in simulations. As a result, the simulation data will demonstrate which is the best control method. To guarantee the safety and proper generation of electricity, the $q$-axis current is constrained within 20A. The PMLSG parameters are given in Table 1.

**Table 1** Selected parameters of the PMLSG

| Parameter | Symbol | Value | Unit |
|---|---|---|---|
| Stator resistance | $R_s$ | 10.16 | Ω |
| Stator inductance | $L_s$ | 12.78 | mH |
| load resistance | $R$ | 10 30 60 | Ω |
| Numbers of pole pairs | $n_p$ | 7 | |
| PM flux | $\Psi$ | 0.625 | Wb |
| Pole pitch | $\tau$ | 71.2 | mm |
| Frictional coefficient | $B_v$ | 0.0006 | Nm/s |
| Max velocity | $v$ | 2.6 | m/s |
| Mass | $M$ | 3.75 | Kg |
| DC-link voltage | $U_{dc}$ | 380 | V |
| Sampling period | $T_s$ | 1e-5 | s |

The tradition FOC extends to three PI controllers, one is voltage loop and two are current loops. The method involved in [6] is adopted to obtain the parameters of the PI controllers. Table 2 lists the selected PI parameters.

**Table 2** Parameters of the PI controllers

| Controller | P | I |
|---|---|---|
| $U_{dc}$ controller | 0.12 | 7.42 |
| $q$-axis current controller | 6.04 | 68.35 |
| $d$-axis current controller | 5.03 | 84.51 |

To examine and verify the proposed SFC method on the dSPACE platform, the model is discretized. The proposed SFC method is shown by the block diagram in Fig.4(a). $\boldsymbol{K}_{dx}$ and $\boldsymbol{K}_{de}$ are elements of gain matrix which can be calculated in MATLAB by utilizing the following formula:

$$[k,\sim,\sim]=LQR(\boldsymbol{A},\boldsymbol{B},\boldsymbol{Q},\boldsymbol{R}) \tag{27}$$

The nonlinear parts are given from the (3)

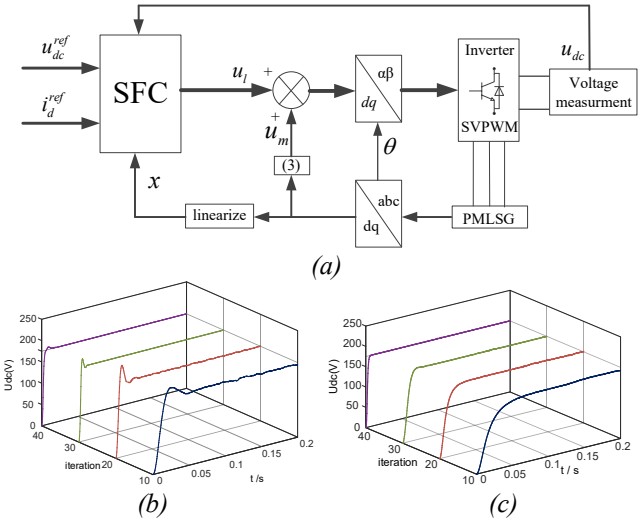


***Fig. 4.*** ***(a)*** *Block diagram of PMLSG with proposed SFC,* ***(b)*** *Variation of Udc during auto-tuning procedure with* $F_1$*,* ***(c)*** *Variation of* $U_{dc}$ *during auto-tuning procedure with* $F_2$

Firstly, the parameters of GWO algorithm will be chosen to start the optimization process. The population of grey wolves may affect the searching time and complexity of the optimization directly. Although more wolves can find the optimal gain matrix, the more time needs to be consumed. The number of wolves and maximum iterations are picked 30. The upper boundary is selected as $1\times10^{6}$ and the lower boundary is selected as $1\times10^{-3}$. Figs.4(b) and (c) demonstrate the evolution of direct voltage during the auto-tuning procedure ($U_{dc}$=175V, $R$=10Ω). In order to investigate how the GWO algorithm iteration number influences the early stage convergence and how the objective function parameters are selected to reduce the steady-error and improve dynamic response, simulation about auto-tuning procedure is carried out in Fig.5. It affirms the overall trend of fitness values corresponding to the iteration number during GWO procedure, respectively. Because of the existence of penalty term, the initial value of $F_2$ is very large, and it decreases rapidly with the following iterations. When the iteration times arrive 28 times, the difference between $F_1$ and $F_2$ has become relatively small, and after 40 iterations, they get closer and closer in general. The best fitness indexes after 40 iterations are $F_1$=4.434 and $F_2$=4.429, respectively. Considering this result, the iteration number is chosen equal to 40, which satisfies both convergence precision and minimizes time calculation real time implementation.

**Table 3** Selected parameters of GWO algorithm

| Parameter | Symbol | Value |
|---|---|---|
| Number of wolves | $n$ | 30 |
| Maximum iterations | $m$ | 40 |
| Upper bounds | $u_b$ | $1\times10^{6}$ |
| Lower bounds | $l_b$ | $1\times10^{-3}$ |

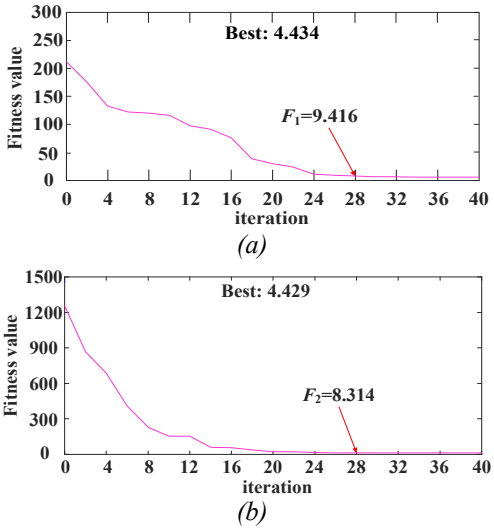


***Fig. 5.*** ***(a)*** *Variation of* $F_1$ *during auto-tuning procedure,* ***(b)*** *Variation of* $F_2$ *during auto-tuning procedure*

What is more, Matrices $\boldsymbol{Q}$ and $\boldsymbol{R}$ calculated by GWO have an influence on state tracking error and control energy loss in PMLSG control process. Weighting factor is represented by the main diagonal elements of the matrix $\boldsymbol{Q}$, which shows the relative importance of each index error. The effect of control signals is compared by $r_1$ and $r_2$. After 40 iterations the final values of weighting matrices are obtained as follows.

$$\boldsymbol{Q}_1=\begin{bmatrix}108.4&0&0&0&0\\0&3.18&0&0&0\\0&0&0.62&0&0\\0&0&0&37.64&0\\0&0&0&0&29.03\end{bmatrix},\boldsymbol{R}_1=\begin{bmatrix}1e-3&0\\0&47.3\end{bmatrix}$$

$$\boldsymbol{Q}_2=\begin{bmatrix}75.8&0&0&0&0\\0&1.56&0&0&0\\0&0&0.10&0&0\\0&0&0&62.56&0\\0&0&0&0&10.21\end{bmatrix},\boldsymbol{R}_2=\begin{bmatrix}1e-3&0\\0&52.63\end{bmatrix}$$

The relative gain matrices are:

$$\boldsymbol{K}_1=\begin{bmatrix}320.6&0&0&0&168.42\\0&1.70&0.0423&0.7661&0\end{bmatrix}$$

$$\boldsymbol{K}_2=\begin{bmatrix}280.64&0&0&0&100.55\\0&1.46&0.05&1.14&0\end{bmatrix}$$

The performance of the PMLSG generating electricity are researched at different load resistances. The comparisons are made to show the difference among classical FOC method (PI controllers), the SFC controller with objective function $F_1$ and the SFC controller with objective function $F_2$. The following Figs.6, 7 and 8. demonstrate the dynamic properties of the tradition PI controller, SFC1 and SFC2 at 10, 30 and 60Ω, respectively. Since the maximum direct voltage is 380V, we set $U_{dc}^{ref}$=175V for different load resistance. In order to compare with different load resistances, the velocity is set the same and the torque is set 30Nm to simulate the ocean energy.

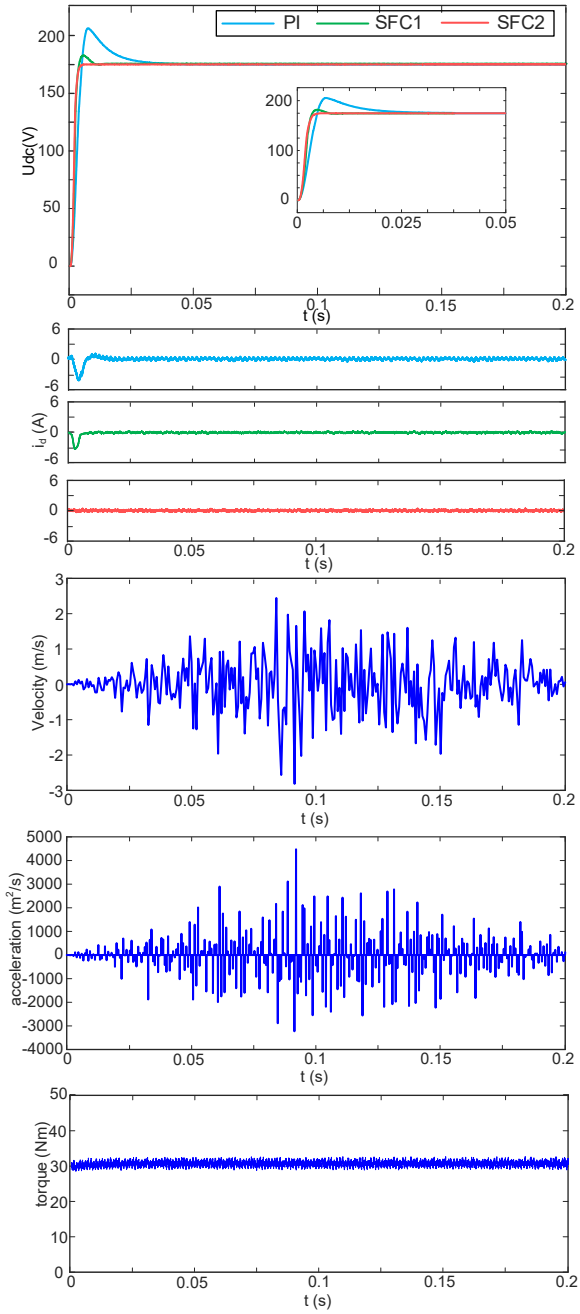


***Fig. 6.*** *Simulation response of PMLSG at 10Ω resistance direct voltage, d-axis current, velocity, acceleration, torque*

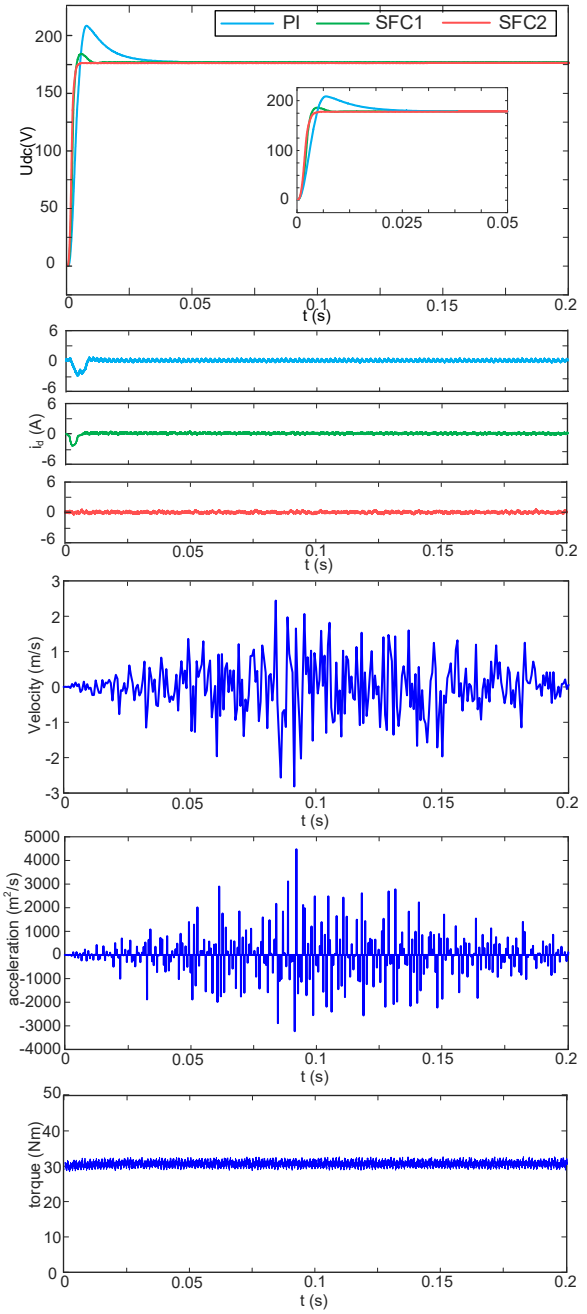


***Fig. 7.*** *Simulation response of PMLSG at 30Ω resistance direct voltage, d-axis current, velocity, acceleration, torque*

### *6.1. At 10Ω Load Resistance Condition*

The velocity, acceleration and torque provided by motive power are shown in Fig.6. When load resistance is 10Ω, all the three methods of generator can track reference voltage without steady-state error. As shown in Fig.6, the generation with PI control has a relatively large overshoot, and generation based on SFC1 can reduce it greatly. As can be seen, owing to the introduction of penalty term $\eta$ in (22), it allows tracking reference voltage almost without overshoot. What is more, under the load resistance, voltage can reach the stead state faster with SFC1 and SFC2 than PI controller. The reference value of $i_d$ is set zero at first in this experiment. Thanks to the second part in fitness index, SFC1 and SFC2 have more subtle vibration in $i_d$ at steady state than PI.

### *6.2. At 30Ω Load Resistance Condition*

In this section, the resistance is changed to 30Ω in the whole period simulation. The responses of the output direct voltage, *d*-axis current, velocity, acceleration and torque are shown in Fig.7. The time of going up and reaching steady state with PI controllers are relatively longer on contrast to the 10Ω load resistance condition. Therefore, the advantage of SFC1 and SFC2 in larger load resistance is documented. The application of two state feedback control has reduced the rise time of direct voltage generated by PMSLG. The value of rise time has decreased almost 23.4% and 18.4%, respectively. What is more, SFC1 results in 1.91% overshoot in PMLSG output voltage, but SFC2 eliminates the overshoot completely.

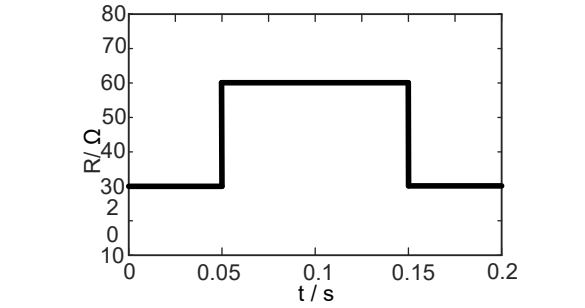


*(a)*

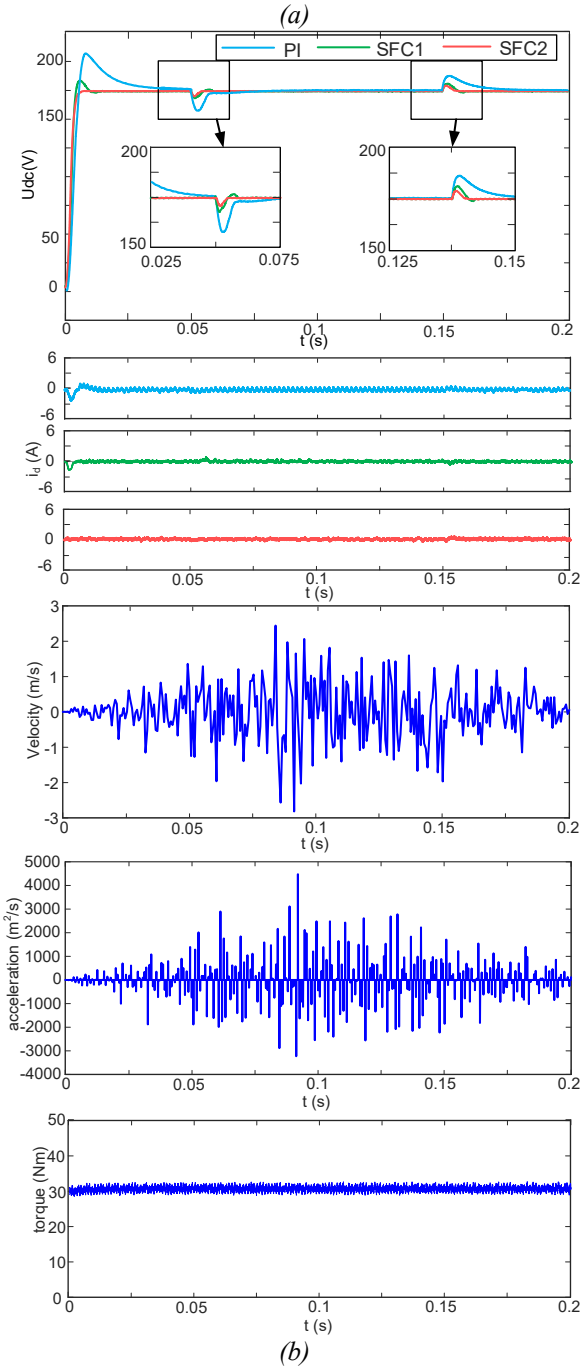


*(b)*

***Fig. 8.*** ***(a)*** *Load resistance, Simulation responses of PMLSG generating at variable load conditions* ***(b)*** *direct voltage, d-axis current, velocity, acceleration, torque*

### *6.3. At Variable Load Resistance Condition*

In this part, the load resistance is initially set to 30Ω. When the PMLSG generates stably at voltage of 175V, the load resistance is changed from 30Ω to 60Ω. The transformation is applied to test the disturbance rejection performance, as show in Fig.8(a), and the responses of the direct voltage, *d*-axis current, velocity, acceleration and torque are shown in Fig.8(b). It can be observed that the steady-state tracking errors of the PI, SFC1 and SFC2 are all zero error under disturbance existence, and the value of d-axis current has no fluctuation during the variation of load resistance.

When the load resistance is applied, PI based on generation leads to 8.25% decline in voltage and takes 0.01s to stabilize the system again. SFC1 associated with GWO offers 63% reduction in voltage drop and 72% reduction in settling time of the PMLSG. SFC2 caused to 68% reduction in voltage drop and 80% faster settling time of PMSLG voltage. It is evident that compared with the classical PI based FOC method, the SFC generation based on GWO is much more efficient in voltage control of PMLSG. In addition, SFC2 has smaller overshoot and a slightly worse load resistance compensation compared to SFC1 controller.

## 7. Experiment Results

Several experiments are put into effect to verify the system performance. The experimental equipment is installed in Fig.9. The test bench contains a PMLSG and a motive power and the parameter of PMLSG is the same as Table 1.

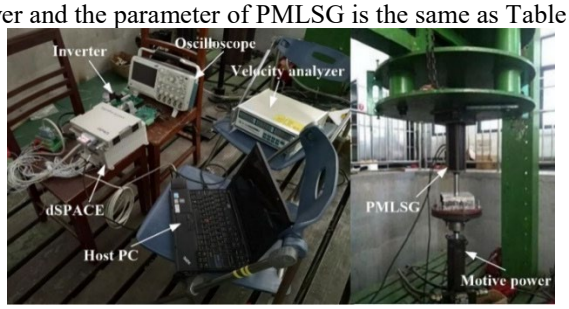


***Fig.9.*** *Experimental outfit*

The proposed control scheme is realized in a dSPACE DS1401 PPC. Compared with the simulation results intuitively, the experiment uses the same values of reference direct voltage and load resistance. The torque is set 30Nm and the velocity is set within 2.6 m/s to simulate the ocean energy.

The experimental responses of the PMLSG with different controllers under 10Ω load resistance, 30Ω load resistance and variable load resistance conditions are revealed in Figs.10- 12, respectively. The velocity, acceleration and torque are also shown in Figs.10-12. It can be noted that the response of the PMSLG conforms to the simulation results given in Figs.6, 7 and 8. As can been see, steady state error free operation come true with all controllers in experiment Figs.10-12. What is more, better compensation of external load resistances is noticed with SFC1 and SFC2 controllers. In addition of the direct voltage, *d*-axis current maintains zero at steady state with all control strategies, but the initial current conditions of different controllers have different effects. The SFC1 and SFC2 controllers have clearly advantages in reducing current oscillation. The noise of *d*-axis current in SFC1 and SFC2 is mainly affected by the value of $\boldsymbol{K}_{dx1}$ obtained from auto-tuning process. With the help of penalty term in objective function, the direct voltage drops and overshot with SFC2 controller are the smallest when adding the different load resistances.

A series of index including rise time, peak overshoot, peak time and settling time, are reported for 10Ω load and 30Ω load resistance conditions in Table 4. In Table 5,

different indicators such as speed drop, peak overshoot and transient time are shown in variable load resistance condition. As it can be appreciated, the strengths and weaknesses of every controller are reflected.

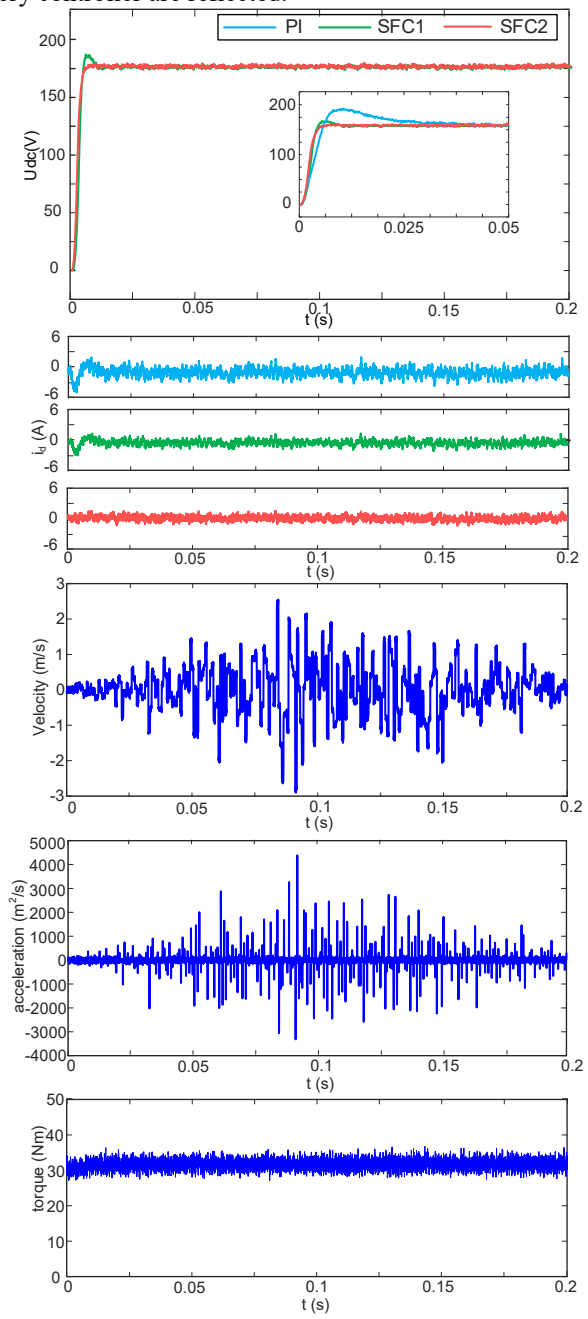


*Fig. 10. Experimental responses of PMLSG generating at 10Ω resistance direct voltage, d-axis current, velocity, acceleration, torque*

**Table 4** Dynamic response of PMLSG at 10Ω load resistance and 30Ω load resistance conditions

| Methods | Load conditions | Rise time (ms) | Peak overshoot (%) | Peak time (s) | Settling time (s) |
|---|---|---|---|---|---|
| PI | 10Ω load | 4.2 | 17.8 | 0.01 | 0.06 |
| | 30Ω load | 10 | 15.5 | 0.015 | 0.071 |
| SFC1 | 10Ω load | 3.2 | 4.2 | 0.006 | 0.012 |
| | 30Ω load | 9 | 3.3 | 0.008 | 0.03 |
| SFC2 | 10Ω load | 3.8 | - | - | 0.0062 |
| | 30Ω load | 10.2 | - | - | 0.0083 |

**Table 5** Dynamic response of PMLSG at variable load conditions

| Load conditions | Generation Characteristic | PI | SFC1 | SFC2 |
|---|---|---|---|---|
| Load increased | Speed drop (%) | 12.5 | 6.1 | 4.3 |
| | Transient time (ms) | 25 | 9.5 | 6 |
| Load decreased | Peak overshoot (%) | 10.2 | 6.5 | 4 |
| | Transient time (ms) | 30 | 9.2 | 6.4 |

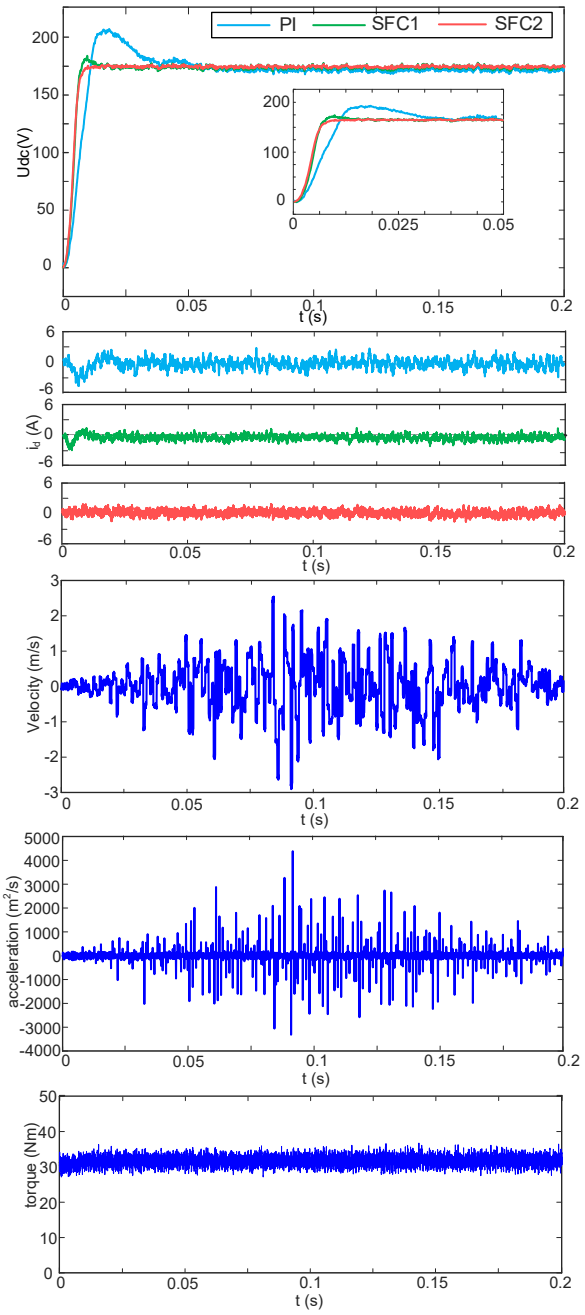


*Fig. 11. Experimental responses of PMLSG generating at 30Ω resistance direct voltage, d-axis current, velocity, acceleration, torque*

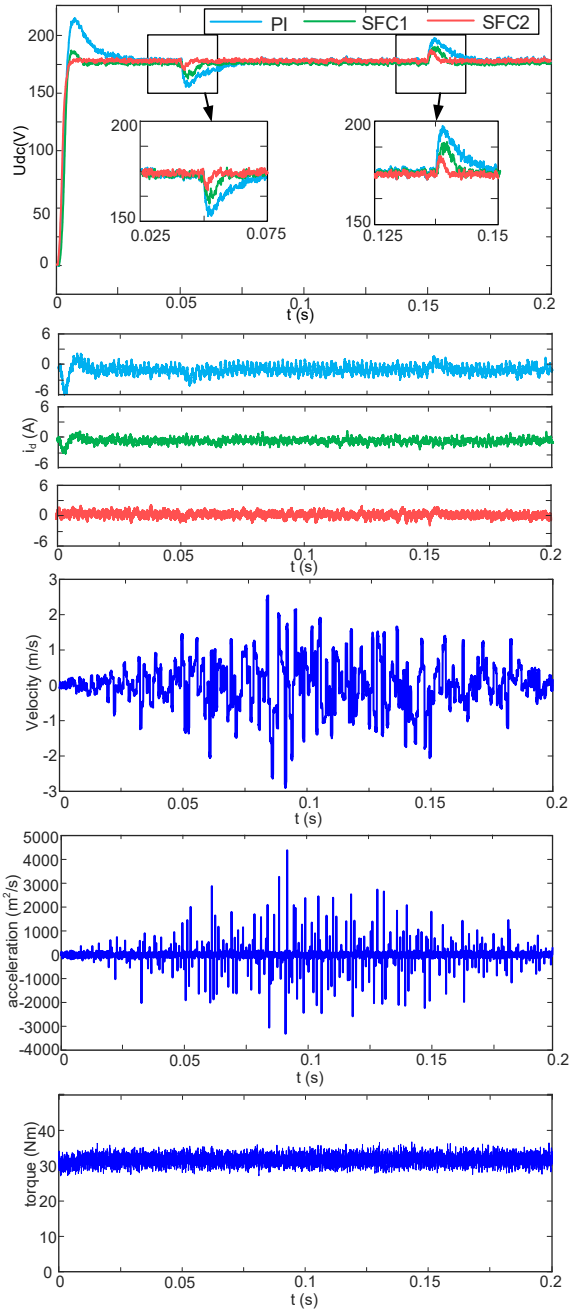


***Fig. 12.*** *Experimental responses of PMLSG generating at variable load resistances, direct voltage, d-axis current, velocity, acceleration, torque*

## 8. Conclusion

This paper has proposed a GWO based on state feedback control for high performance control of PMLSG generation. Depending on the proposed controller, the satisfactory property of direct voltage under variable resistance is obtained. A MIMO nonlinear state-space of PMLSG is given first. Then, a critical step is taken to linearize the model. Integral action of tracking speed and zero *d*-axis current are incorporated in the control scheme by state augmentation of the novel state-space model to reduce the steady-state error. The GWO algorithm plays an important role in acquiring values of weighting matrices ***Q*** and ***R*** which are demanded to calculate discrete state feedback voltage controllers by Matlab LQR function. The overshoot produced by weighting matrices can be filtered out in effect of a penalty term that was introduced into the fitness index. In addition, comparative researches including a PI controller, SFC without penalty term and SFC with penalty term of objective function were implemented under dSPACE 1401 control board, and the end-results underlined the improvement of the proposed state feedback controller.

## 9. References


[1] Sun, X., Diao, K., and Yang, Z.: 'Performance improvement of a switched reluctance machine with segmental rotors for hybrid electric vehicles', *Comput. Electr. Eng.*, 2019, **77**, pp. 244-259

[2] Huang, L., Yu, H., Hu, M., Zhao, J., and Cheng, Z.: 'A novel flux-switching permanent-magnet linear generator for wave energy extraction application', *IEEE Trans. Magn.,*2011, **47**,( 5), pp. 1034-1037

[3] Davidson, J., Genest, R., and Ringwood, J. V.: 'Adaptive Control of a Wave Energy Converter', *IEEE Trans. Sustain Energ.,* 2018, **9**, (4), pp. 1588-1595

[4] Huang, L., Hu, M., Yu, H., Liu, C., and Chen, Z.: 'Design and experiment of a direct-drive wave energy converter using outer-PM linear tubular generator', *IET Renew Power Gen.,* 2017, **11**, (3), pp. 353-360

[5] Sun, X., Diao, K., Lei, G., Guo, Y., and Zhu, J.: 'Real-time HIL emulation for a segmented-rotor switched reluctance motor using a new magnetic equivalent circuit', *IEEE Trans. Power Electron.*, 2019, DOI: 10.1109/TPEL.2019.2933664.

[6] Oh, J., Park, J. S., Hyon, B. J., and Lee, J.: 'Novel control strategy of wave energy converter using linear permanent magnet synchronous generator', *IEEE Trans. Appl. Supercon.,* 2018, **28**, (3), pp. 1-5

[7] Son, D. and Yeung, R. W.: 'Real-time implementation and validation of optimal damping control for a permanent-magnet linear generator in wave energy extraction', *Appl Energ*., 2017, **208**, pp. 571-579

[8] Sun, X., Diao, K., Lei, G., Guo, Y., and Zhu, J.: 'Study on segmented-rotor switched reluctance motors with different rotor pole numbers for BSG system of hybrid electric vehicles', *IEEE Trans Veh. Technol.*, 2019, **68**, (6), pp.5537-5547

[9] Zhu, X., Huang, J., Quan, L., Xiang, Z., and Shi, B.: 'Comprehensive sensitivity analysis and multi-objective optimization research of permanent magnet flux-intensifying motors', *IEEE Trans. Ind. Electron*., 2019,**66**, (4), pp. 2613-2627

[10] Sun, X., Shen, Y., Wang, S., Lei, G., Yang, Z., and Han, S.: 'Core losses analysis of a novel 16/10 segmented rotor switched reluctance BSG motor for HEVs using nonlinear lumped parameter equivalent circuit model', *IEEE/ASME Trans. Mechatron.*, 2018, **23**, (2), pp. 747-757

[11] Zhu, X., Wu, W., Quan, L., Xiang, Z., and Gu, W., 'Design and multi-objective stratified optimization of a less-rare-earth hybrid permanent magnets motor with high torque density and low cost', *IEEE Trans. Energy Convers.,* 2019,**34**, (3), pp. 1178-1189

[12] Du, C., Yin, Z., Zhang, Y., Liu, J., Sun, X., and Zhong, Y.: 'Research on active disturbance rejection control with parameter autotune mechanism for induction motors based on adaptive particle swarm optimization algorithm with dynamic inertia weight', *IEEE Trans. Power Electron.,* 2019., 34, (3), pp. 2841-2855

[13] Faa-Jeng, L., Syuan-Yi, C., Li-Tao, T., and Hen, C.: 'Recurrent functional-link-based fuzzy neural network controller with improved particle swarm optimization for a linear synchronous motor drive', *IEEE Trans. Magn.,* 2009, **45**, (8), pp. 3151-3165

[14] Sun, X., Shi, Z., Lei, G., Guo, Y., and Zhu, J.: 'Analysis, design and optimization of a permanent magnet synchronous motor for a campus patrol electric vehicle', *IEEE Trans. Veh. Technol*, 2019,**68**, (11), pp. 10535-10544

[15] Liu, Z. H., Zhang, J., Zhou, S. W., Li, X. H., and Liu, K.: 'Coevolutionary particle swarm optimization using AIS and its application in multiparameter estimation of PMSM', *IEEE Trans Cybern.,* 2013, **43**, (6), pp. 1921-1935

[16] Sun, X., Diao, K., Yang, Z., Lei, G., Guo, Y., and Zhu, J.: 'Direct torque control based on a fast modeling method for a segmented-rotor switched reluctance motor in HEV application', *IEEE J. Emerg. Sel. Topics Power Electron.,* 2019, DOI: 10.1109/JESTPE.2019.2950085

[17] Hao, W., Ma, C., Moghimi, B., Fan, Y., and Gao, Z.: 'Robust optimization of signal control parameters for unsaturated intersection based on tabu search-artificial bee colony algorithm,' *IEEE Access,* 2018, **6**, pp. 32015-32022

[18] Tarczewski, T., and Grzesiak, L. M.: 'An application of novel nature-inspired optimization algorithms to auto-tuning state feedback speed controller for PMSM,' *IEEE Trans. Ind. Appl.,* 2018, **54**, (3), pp. 2913-2925

[19] Mirjalili S, Mohammad S, and Lewis A,: 'Grey wolf optimize,' *Advances in Engineering Software.*, 2014, **69**, (3), pp. 46–61

[20] Chaman-Motlagh, A.: 'Superdefect photonic crystal filter optimization using grey wolf optimizer,' *IEEE Photonic Tech L.,* 2015, **27**, (22), pp. 2355-2358

[21] Precup, R.-E., David, R.-C., and Petriu, E. M.: 'Grey wolf optimizer algorithm-Based tuning of fuzzy control systems with reduced parametric sensitivity', *IEEE Trans. Ind. Electron.,* 2017. **64**, (1), pp. 527-534

[22] Sun, X., Jin, Z., Wang, S., Yang, Z., Li, K., Fan, Y. and Chen, L.: 'Performance improvement of torque and suspension force for a novel five-phase BFSPM machine for flywheel energy storage systems', *IEEE Trans. Appl. Supercon.*, 2019, **29**, (2), Art. no.: 0601505

[23] Zhu, X., Fan, D., Xiang, Z., Quan, L., Hua, W., and Cheng, M.: 'Systematic multi-level optimization design and dynamic control of less-rare-earth hybrid permanent magnet motor for all-climatic electric vehicles', *Applied Energy*, DOI: 10.1016/j.apenergy.2019.113549

[24] Sun, X., Cao, J., Lei, G., Guo, Y., and Zhu, J.: 'Speed sensorless control for permanent magnet synchronous motors based on finite position set', *IEEE Trans. Ind. Electron.,* 2019, DOI: 10.1109/TIE.2019.2947875

[25] Tarczewski Tomasz, and M. Grzesiak Lech.: 'Constrained state feedback speed control of PMSM based on model predictive approach,' *IEEE Trans. Ind. Electron.,* 2016, **63,** (6), pp. 3867-3875

[26] Brasel, M.: 'A gain-scheduled multivariable LQR controller for permanent magnet synchronous motor, ' in *Proc. 19th Int. Conf. Methods Models Auto. Robot. (MMAR)*, 2014, pp. 722-725

[27] Xia, C., Liu, N., Zhou, Z., Yan, Y., and Shi, T.: 'Steady-state performance improvement for LQR-based PMSM drives,' *IEEE Trans. Power Electron.,* 2018, **33**, (12), pp. 10622-10632

[28] Cheema, M. A. M., Fletcher, J. E., Xiao, D., and Rahman, M. F.: 'A linear quadratic regulator-based optimal direct thrust force control of linear permanent-magnet synchronous motor,' *IEEE Trans. Ind. Electron.,* 2018, **63**, (5), pp.2722-2733

[29] Zhu, X., Jiang, M., Xiang, Z., Quan, L., Hua, W., and Cheng, M.: 'Design and optimization of a flux-modulated permanent magnet motor based on an airgap-harmonic-orientated design methodology', *IEEE Trans. Ind. Electron.*, DOI: 10.1109/TIE.2019.2934063

[30] Sun, X., Hu, C., Lei, Gang, Guo, Y., and Zhu, J.: 'State feedback control for a PM hub motor based on grey wolf optimization algorithm', *IEEE Trans. Power Electron.*, 2020, **35**, (1), pp. 1136-1146